BIOCHEMISTRY

Key determinants of selective binding and activation by the monocyte chemoattractant proteins at the chemokine receptor CCR2

Zil E. Huma,[1] Julie Sanchez,[1] Herman D. Lim,[2] Jessica L. Bridgford,[1,2] Cheng Huang,[1] Bradyn J. Parker,[1] Jiann G. Pazhamalil,[1] Benjamin T. Porebski,[1] Kevin D. G. Pfleger,[3] J. Robert Lane,[2] Meritxell Canals,[2]* Martin J. Stone[1]*

Chemokines and their receptors collectively orchestrate the trafficking of leukocytes in normal immune function and inflammatory diseases. Different chemokines can induce distinct responses at the same receptor. In comparison to monocyte chemoattractant protein-1 (MCP-1; also known as CCL2), the chemokines MCP-2 (CCL8) and MCP-3 (CCL7) are partial agonists of their shared receptor CCR2, a key regulator of the trafficking of monocytes and macrophages that contribute to the pathology of atherosclerosis, obesity, and type 2 diabetes. Through experiments with chimeras of MCP-1 and MCP-3, we identified the chemokine amino-terminal region as being the primary determinant of both the binding and signaling selectivity of these two chemokines at CCR2. Analysis of CCR2 mutants showed that the chemokine amino terminus interacts with the major subpocket in the transmembrane helical bundle of CCR2, which is distinct from the interactions of some other chemokines with the minor subpockets of their receptors. These results suggest the major subpocket as a target for the development of small-molecule inhibitors of CCR2.

INTRODUCTION

Heterotrimeric guanine nucleotide–binding protein (G protein)–coupled receptors (GPCRs) are the largest family of transmembrane (TM) receptors and the targets of numerous therapeutics. Many GPCRs can be activated by various different natural or synthetic agonists, which may give rise to distinct signaling outcomes. Whereas partial agonists evoke a submaximal response relative to that of a full agonist even at concentrations that saturate all receptor sites, biased agonists can display pathway-dependent efficacy, activating certain pathways to the relative exclusion of others (*1*, *2*).

The recent flood of GPCR structures has yielded a wealth of information regarding receptor architecture, ligand-binding sites, and G protein–binding sites, as well as some details of the conformational changes associated with receptor activation (*3*–*5*). Consequently, we can now begin to identify the structural mechanisms by which different agonists induce distinct signaling outcomes. Here, we describe an analysis of the structural features underlying differential activation of a chemokine receptor by its cognate chemokine ligands.

Chemokine receptors are GPCRs expressed in leukocyte membranes, whereas chemokines are small, soluble proteins expressed in tissues during normal immune surveillance or in response to injury or infection. Activation of chemokine receptors by their cognate chemokines induces leukocyte migration into, and accumulation in, the chemokine-expressing tissues (*6*–*8*), a hallmark feature of the inflammatory response. Consequently, chemokine receptors are potential therapeutic targets in a wide range of inflammatory diseases (*9*). There is increasing evidence that cognate chemokines can differentially activate their shared receptors, including examples of partial agonism (*10*–*14*) and biased agonism (*15*, *16*).

CC chemokine receptor 2 (CCR2) is the major chemokine receptor on monocytes and macrophages, cells that play central roles in the pathology of atherosclerosis, obesity, and type 2 diabetes. In atherosclerosis, CCR2 activation by the monocyte chemoattractant proteins MCP-1, MCP-2, and MCP-3 induces the recruitment of monocytes from the blood into the arterial walls, where they differentiate into macrophages and contribute to the development of atherosclerotic plaques (*17*). In obesity, CCR2 activation by MCP chemokines is associated with macrophage infiltration into adipose tissue and induction of insulin resistance (*18*). Considering the importance of CCR2 in inflammatory diseases, there is strong motivation to understand its mechanism of activation by its cognate chemokine ligands.

Although their distinct biological functions are not fully understood, the MCP chemokines are differentially expressed in response to type 1 versus type 2 T helper cell inflammatory stimuli and can have distinct temporal patterns of expression, suggesting that they may also activate distinct cellular responses through their shared receptor (*19*, *20*). In support of this possibility, Berchiche *et al.* (*13*) showed that cognate chemokines for CCR2 display differences in their efficacies of activation of both β-arrestin– and G protein–mediated signaling pathways. Here, we verified that this differential signaling can be attributed to partial agonism rather than biased agonism, and we used various chemokine chimeras and CCR2 mutants to identify key structural elements of both the chemokines and the receptor that mediate this differential activation. We interpreted our data in light of the published structures of chemokine-receptor complexes (*21*, *22*), yielding insights into the design of selective pharmacological agents.

RESULTS

MCP chemokines have different efficacies and affinities at CCR2

We monitored the activation of CCR2 by MCP chemokines using one proximal, nonamplified measure of receptor activation [recruitment of

[1]Infection and Immunity Program, Monash Biomedicine Discovery Institute, and Department of Biochemistry and Molecular Biology, Monash University, Clayton, Victoria 3800, Australia. [2]Drug Discovery Biology, Monash Institute of Pharmaceutical Sciences, Monash University, Parkville, Victoria 3052, Australia. [3]Molecular Endocrinology and Pharmacology, Harry Perkins Institute of Medical Research, QEII Medical Centre; and Centre for Medical Research, University of Western Australia, Crawley and Dimerix Bioscience Limited, Nedlands, Western Australia, Australia. *Corresponding author. Email: martin.stone@monash.edu (M.J.S.); meri.canals@monash.edu (M.C.)

β-arrestin 2 (β-arr2)] and two downstream, amplified signals [inhibition of adenosine 3′,5′-monophosphate (cAMP) formation and phosphorylation of extracellular signal–regulated kinases 1 and 2 (ERK1/2)]. The three chemokines induced recruitment of β-arr2 with different potencies and statistically significantly different maximal effects, E_{max} ($P < 0.01$; Fig. 1A and Table 1); relative to MCP-1, the E_{max} values of MCP-2 and MCP-3 were 23 ± 3% and 56 ± 4%, respectively. In the two amplified signaling assays, the three chemokines exhibited the same maximal effects but statistically significantly different potencies and higher potencies than in the β-arr2 assay (Fig. 1, B and C, and Table 1). The order of potencies between the three agonists in the amplified assays was the same as the order of their maximal effects in the proximal assay. Moreover, the same rank order of binding affinities was also observed in a radioligand-binding assay (Fig. 1D and Table 1). These results are in agreement with the effects of MCP chemokines reported previously (*13*).

Analysis of our data using an approach based on the operational model of agonism (*23*, *24*) indicated that the MCP chemokines did not display biased agonism (fig. S1 and table S1) but instead that MCP-2 and MCP-3 are partial agonists of CCR2, relative to MCP-1. Our data (Fig. 1, A to D) highlight two underlying differences in the receptor interactions of the MCP chemokines. First, the three chemokines have different affinities for CCR2 (Fig. 1D). Second, the three chemokines had different maximal effects in the proximal β-arr2 recruitment assay (Fig. 1A). Although the rank order of these maximal effects is the same as the rank order of affinities for the three chemokines, the maximal effects occur at ligand concentrations at which the receptor is fully occupied, so they do not result from differences in binding affinity. Instead, they indicate that the ligands have distinct efficacies, that is, distinct intrinsic abilities to induce the receptor-mediated response. In the amplified assays (inhibition of cAMP and ERK1/2 phosphorylation), the maximal effects of full and partial agonists were indistinguishable (the signals were amplified to the full capacity of the pathway even when the activated state of the receptor was only partially populated). In such assays, the relative potency of the chemokines is determined by both the affinities of the chemokines for CCR2 and their relative efficacies (*25*). The order of potency in the cAMP and pERK assays is consistent with both their relative affinities for the receptor and their relative E_{max} values in the proximal assay (Fig. 1, A to D).

An important consequence of partial agonism in the context of the β-arrestin assay is that subsequent regulatory processes, such as receptor internalization, will also be submaximally engaged by the action of partial agonists. In agreement with the work of Berchiche *et al.* (*13*), both MCP-2 and MCP-3, at saturating concentrations, caused very limited internalization of CCR2, whereas MCP-1 stimulated statistically significant internalization ($P < 0.05$; Fig. 1E). These differences correlate with the relative efficacies of the three chemokines. Considering the robust and consistent differences observed among the MCP chemokines for CCR2 binding and activation (Fig. 1), this system is suitable for the investigation of the structural features influencing the relative affinities and efficacies of different chemokines at their shared receptor.

The chemokine N-terminal tail is a major determinant of affinity and efficacy

Mutational and structural studies have identified three regions of chemokines that interact with receptors (*26*–*29*). The so-called N-loop (a ~12-residue sequence between the conserved CC or CXC motif and the first β-strand) and the β3 region (third β-strand and preceding turn) form the two sides of a shallow groove that binds to the flexible N-terminal tail of the receptor. The N-terminal region of the chemokine (preceding the CC or CXC motif) penetrates into the TM helical bundle of the receptor. To identify the structural elements of MCP chemokines that contribute to partial versus full agonism and to relative CCR2 affinity, we prepared a series of chimeras in which these three functionally important regions are swapped between MCP-1 and MCP-3 (Fig. 2). MCP-3, rather than MCP-2, was chosen primarily because it is more closely related to MCP-1, thereby simplifying the interpretation of the chimera experiments. Each chimera was named according to the parental chemokine from which it was derived followed by a sequence of three numbers representing the origin of the N-terminal, N-loop, and β3 elements, respectively; for example, MCP1-133 is a chimera derived from MCP-1 and containing the N-terminal region of MCP-1, the N-loop of MCP-3, and the β3 region of MCP-3. Each chimera was expressed as inclusion bodies in *Escherichia coli*, refolded, and purified. ^{1}H nuclear magnetic resonance (NMR) spectra (Fig. 2 and fig. S2) were similar to those of the wild-type (WT) chemokines, indicating that the chimeras were well folded and adopted the expected native three-dimensional (3D) structures.

To assess the contributions of the three chemokine structural regions to CCR2 binding affinity, we measured the abilities of the MCP chimeras to compete with ^{125}I–MCP-1 for binding to CCR2. MCP-1 had a 10-fold higher affinity than that of MCP-3 for CCR2 (Fig. 3, A and B, and Table 2). Replacement of the N terminus of MCP-1 with that of MCP-3 caused a decrease in affinity such that this chimeric chemokine displayed an affinity comparable to that of MCP-3. Similarly, replacement of the N terminus of MCP-3 with that of MCP-1 generated a chimeric chemokine with comparable affinity to that of MCP-1. These results indicate that the N terminus of MCP-1 has a substantial role in determining its higher affinity for CCR2 compared to that of MCP-3. In contrast to the clear contribution of the N-terminal region to binding selectivity, replacement of the N-loop, β3 region, or both of MCP-1 with those of MCP-3 did not affect the binding affinity for CCR2 (Fig. 3, A and B). Similarly, substitution of the β3 region of MCP-3 with that of MCP-1 had no substantial effect on affinity. However, replacement of the N-loop of MCP-3 by that of MCP-1, alone or in combination with the β3 region (chimeras MCP3-313 and MCP3-311), reduced the affinity for CCR2. This not only is consistent with the previous findings that the N-loop is a major contributor to CCR2 binding but also suggests that the ability of the N-loop to interact favorably with the receptor is dependent on the background scaffold in which it is located. Notably, subsequent introduction of the MCP-1 N-terminal region, resulting in the MCP3-111 chimera, increased its affinity for CCR2 100-fold relative to that of MCP3-311, again highlighting the importance of the N terminus as a determinant of the affinity of the chemokine for CCR2.

To assess the contributions of the three chemokine structural regions to the efficacy of CCR2 activation, we measured the abilities of the chemokine chimeras to stimulate β-arr2 recruitment (Fig. 3C). As described earlier, MCP-3 displayed a statistically significantly lower maximal effect than did MCP-1 (Figs. 1A and 3, B and C). Replacement of the N-loop, β3 region, or both of MCP-1 with those of MCP-3 (or vice versa) caused no statistically significant changes in E_{max}. In contrast, replacement of the N terminus of MCP-1 with that of MCP-3, alone or in combination with replacement of both the N-loop and β3 region, substantially decreased the maximal effect compared to MCP-1, to a value comparable to the maximal effect of MCP-3. This vital role of the N terminus in determining chemokine efficacy at CCR2 was further highlighted in the reciprocal chimeras, whereby integration of the N terminus of MCP-1 into an MCP-3 background (MCP3-133 and

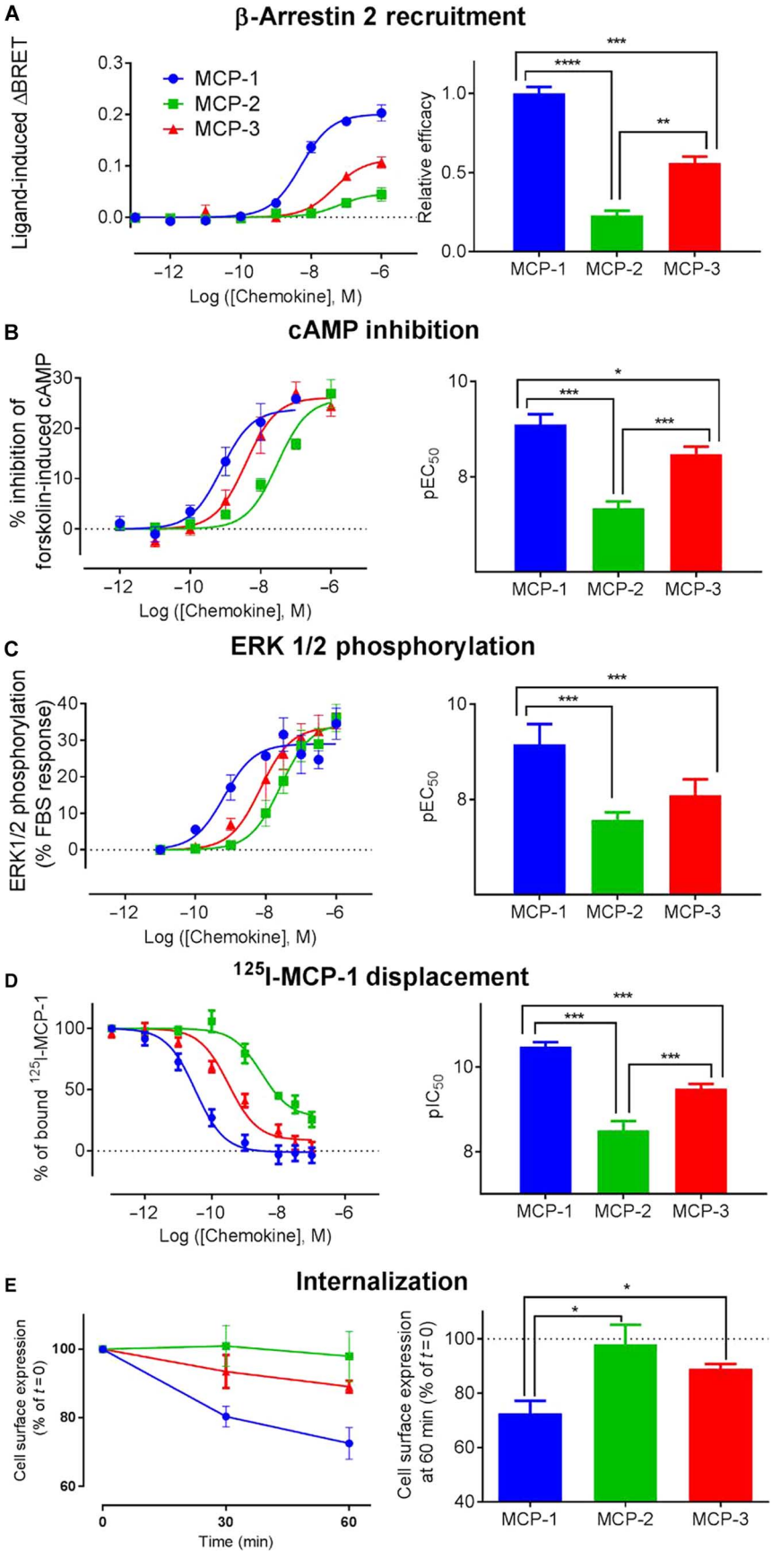

Fig. 1. MCP chemokines display different efficacies and affinities at CCR2. (**A**) Flp-In T-REx 293 cells transiently transfected with plasmids encoding CCR2-RLuc8 and β-arr2–yellow fluorescent protein (YFP) were stimulated with the indicated concentrations of MCP-1, MCP-2, or MCP-3 before being analyzed by BRET to assess the recruitment of β-arr2. Left: Concentration-response data and fitted curves. Right: Relative efficacy, defined as the E_{max} value relative to that of MCP-1. (**B**) c-Myc–FLAG–CCR2 Flp-In T-REx 293 cells transiently transfected with plasmid encoding a BRET-based cAMP sensor were treated with 10 μM forskolin in the presence of the indicated concentrations of chemokines. Left: Measurement of the percentage inhibition of forskolin-stimulated cAMP production as a function of chemokine concentration. Right: Potency (pEC_{50}) values. (**C**) Left: c-Myc–FLAG–CCR2 Flp-In T-REx 293 cells were treated with the indicated concentrations of chemokines for 3 min before the amount of phosphorylated ERK1/2 was measured by AlphaScreen assay. Right: Potency (pEC_{50}) values. (**D**) Left: Membrane preparations of c-Myc–FLAG–CCR2 Flp-In T-REx 293 cells were incubated with 45 pM ^{125}I–MCP-1 in the presence of the indicated concentrations of chemokines before the extent of binding of ^{125}I–MCP-1 was determined by radioligand-binding assay. Right: Affinities (pIC_{50}) for the three chemokines. (**E**) Left: c-Myc–FLAG–CCR2 Flp-In T-REx 293 cells were incubated with 100 nM chemokine for the indicated times before the extent of CCR2 internalization was determined by whole-cell anti–c-Myc enzyme-linked immunosorbent assay (ELISA). Right: Cell surface expression of CCR2 60 min after the addition of chemokine as a percentage of the amount of receptor present immediately before chemokine treatment. Data are means ± SEM of three to five experiments, each performed in triplicate. *$P < 0.05$, **$P < 0.01$, ***$P < 0.001$, and ****$P < 0.0001$ by one-way analysis of variance (ANOVA) with Dunnett's multiple-comparison test.

MCP3-111) resulted in a marked increase in the maximal effect. Furthermore, the E_{max} values of these two chimeras were greater than that of WT MCP-1, again emphasizing that the background chemokine "context" plays an additional role in determining efficacy at CCR2. In addition to the E_{max} values, our data also showed the potencies of the chemokine chimeras in the β-arr2 recruitment assay. Although we observed no statistically significant differences in the potencies (Fig. 3B and Table 2), the rank order of potencies was consistent with those of the binding affinities and E_{max} values. Similarly, at the more amplified signaling end point of ERK1/2 phosphorylation (Fig. 3, B and D), replacing the N terminus of MCP-1 with that of MCP-3 decreased potency, whereas replacing the N terminus of MCP-3 with that of MCP-1 increased potency, although these effects were not statistically significant (Fig. 3B and Table 2).

In the ERK1/2 phosphorylation assay, the two WT chemokines and most chimeras displayed similar maximal effects (Fig. 3, B and D, and Table 2);

Table 1. Potency, efficacy, and affinity of the different MCP chemokines at the CCR2 receptor in β-arrestin recruitment, Fsk-stimulated cAMP inhibition, ERK phosphorylation, and radioligand-binding assays. β-arr2 recruitment was assessed by BRET in Flp-In T-REx 293 cells transiently transfected with plasmids encoding CCR2-RLuc8 and β-arr2–YFP. Inhibition of cAMP was measured in c-Myc–FLAG–CCR2 Flp-In T-REx 293 cells transiently transfected with a plasmid encoding a BRET-based cAMP sensor. ERK1/2 phosphorylation was measured 3 min after c-Myc–FLAG–CCR2 Flp-In T-REx 293 cells were stimulated with chemokine. ^{125}I–MCP-1 competition binding was measured in membrane preparations of c-Myc–FLAG–CCR2 Flp-In T-REx 293 cells. pEC_{50} and pK_i values are the negative log of EC_{50} and inhibition constant (K_i) values, respectively, in molar units. E_{max} values are reported as a percentage of the value for MCP-1. Data are means ± SEM of three or four experiments, each performed in triplicate. *P < 0.05, **P < 0.01, ***P < 0.001 by one-way ANOVA with Dunnett's multiple-comparison test. E_{max} is shown relative to that observed with MCP-1.

	β-Arrestin recruitment		cAMP inhibition		ERK1/2 phosphorylation		^{125}I–MCP-1 binding
	pEC_{50}	E_{max}	pEC_{50}	E_{max}	pEC_{50}	E_{max}	pK_i
MCP-1	8.32 ± 0.06	100 ± 2	9.10 ± 0.21	100 ± 9	9.16 ± 0.24	100 ± 10	10.60 ± 0.08
MCP-2	7.24 ± 0.26*	23 ± 3***	7.34 ± 0.14***	113 ± 9	7.58 ± 0.15***	119 ± 9	8.88 ± 0.14***
MCP-3	7.33 ± 0.15*	56 ± 4**	8.47 ± 0.16*	109 ± 9	8.09 ± 0.19***	116 ± 10	9.50 ± 0.12***

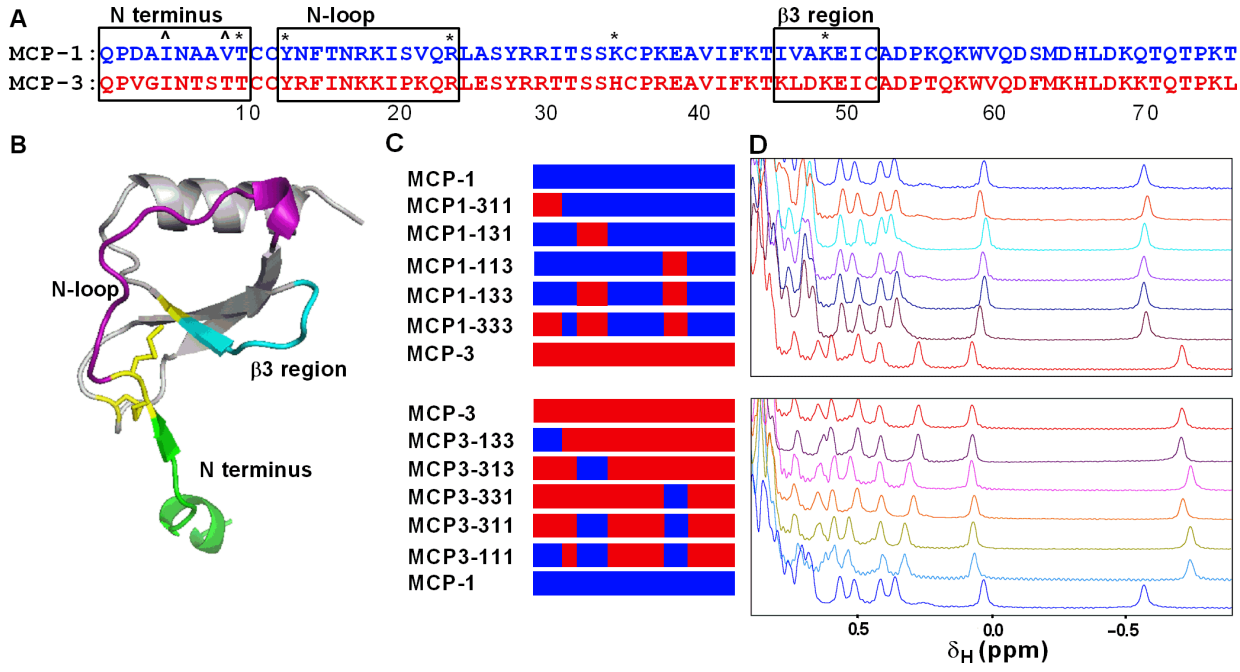

Fig. 2. Design and structural validation of MCP-1/MCP-3 chimeras. (**A**) Aligned sequences of MCP-1 and MCP-3 with the three regions that were swapped in the chimeras indicated by boxes. Symbols above the residue labels indicate those previously found to be important in CCR2 binding (*) or activation (^) (*27*, *28*). (**B**) The structure of MCP-1 (PDB code: 1dok) highlighting the regions swapped in the chimeras. (**C**) Nomenclature and schematic diagrams of the chimeras with regions from MCP-1 and MCP-3 in blue and red, respectively. (**D**) Upfield (methyl) region of the ^{1}H NMR spectra of the WT and chimeric chemokines, showing well-dispersed peaks indicative of correct folding. ppm, parts per million.

however, the MCP3-111 chimera displayed a statistically significantly lower E_{max} than that of WT MCP-3 (P < 0.05) in the ERK1/2 phosphorylation assay despite exhibiting a significantly higher E_{max} than that of MCP-3 in the β-arr2 assay (P < 0.05). Further analysis (fig. S3 and table S2) indicated that this chimera displayed statistically significant biased agonism (P < 0.05) relative to WT MCP-3, suggesting that the three substituted regions of the chemokines may act cooperatively to influence signaling efficacy in a pathway-specific manner. Together, these data indicate that the N termini of MCP-1 and MCP-3 have important roles in determining the relative affinities of the different chemokines at CCR2, as well as their relative efficacies. On the basis of these results, we predicted that the chimeric chemokines in which the N-terminal regions were swapped would have altered abilities to stimulate CCR2 internalization. As expected, MCP1-311 lost its ability to internalize CCR2, whereas the reciprocal N-terminal swap chimera (MCP3-133) stimulated receptor internalization (Fig. 3E).

TM residues of CCR2 contribute to differential chemokine binding and agonism

In light of the observations that the chemokine N-terminal regions contribute to both the affinity of CCR2 binding and the efficacy of CCR2 activation, we sought to identify the residues within CCR2 with which

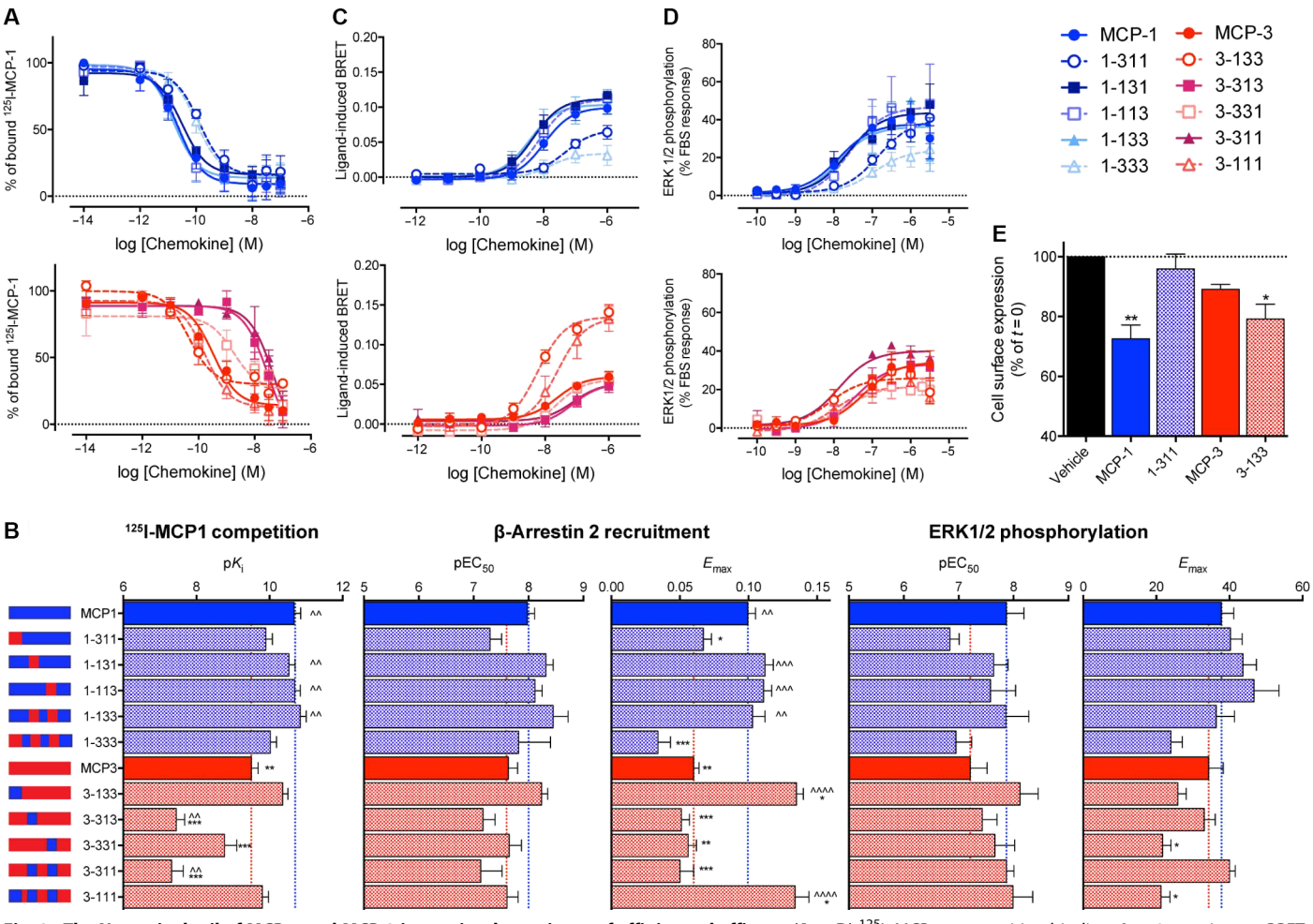

Fig. 3. The N-terminal tail of MCP-1 and MCP-3 is a major determinant of affinity and efficacy. (**A** to **D**) ^{125}I–MCP-1 competition binding, β-arr2 recruitment BRET, and ERK1/2 phosphorylation were assessed for MCP-1 and chimeras in the MCP-1 background (shades of blue) and for MCP-3 and chimeras in the MCP-3 background (shades of red). (A) Membrane preparations of c-Myc–FLAG–CCR2 Flp-In T-REx 293 cells were incubated with 45 pM ^{125}I–MCP-1 in the presence of the indicated concentrations of chemokines before the extent of binding of ^{125}I–MCP-1 was determined by radioligand-binding assay. Top: Competitive displacement data for MCP-1 and chimeras in the MCP-1 background. Bottom: Competitive displacement data for MCP-3 and chimeras in the MCP-3 background. (B) Left: Schematic representations of the WT and chimeric chemokines. As indicated, measurements of the affinity (pK_i) of the indicated chemokines for CCR2, as determined by ^{125}I–MCP-1 competition, the potency (pEC_{50}) and efficacy (E_{max}) of chemokines in the β-arr2 recruitment assay, and the potency (pEC_{50}) and efficacy (E_{max}) of chemokines in the ERK1/2 phosphorylation assay. (C) Flp-In T-REx 293 cells transiently transfected with plasmids encoding CCR2-RLuc8 and β-arr2–YFP were stimulated with the indicated concentrations of WT or chimeric chemokines before being analyzed by BRET to assess the recruitment of β-arr2. Top: Concentration-response data for MCP-1 and chimeras in the MCP-1 background. Bottom: Concentration-response data for MCP-3 and chimeras in the MCP-3 background. (D) c-Myc–FLAG–CCR2 Flp-In T-REx 293 cells were treated with the indicated concentrations of WT or chimeric chemokines for 3 min before the amount of phosphorylated ERK1/2 was measured by AlphaScreen assay. Top: Concentration-response data for MCP-1 and chimeras in the MCP-1 background. Bottom: Concentration-response data for MCP-3 and chimeras in the MCP-3 background. (**E**) c-Myc–FLAG–CCR2 Flp-In T-REx 293 cells were incubated with the indicated chemokine (100 nM) for 60 min before the cell surface expression of CCR2 was determined by whole-cell anti–c-Myc ELISA. Expression is presented as a percentage of that of the vehicle control. Data are means ± SEM of three to five experiments, each performed in triplicate. *P < 0.05, **P < 0.01, ***P < 0.001, and ****P < 0.0001 compared to MCP-1. ^P < 0.05, ^^P < 0.01, ^^^P < 0.001, and ^^^^P < 0.0001 compared to MCP-3. Statistical analysis was by one-way ANOVA with Dunnett's multiple-comparison test.

the chemokine N-terminal regions interact. Published structures of two chemokine-receptor complexes (*21*, *22*) have confirmed that the N-terminal regions of chemokines penetrate into the TM helical bundles of their receptors, where they presumably cause structural rearrangements and signaling. To identify specific residues of CCR2 that contribute to these interactions, we characterized chemokine binding and activation for a series of CCR2 mutants. Guided by a homology model of the MCP-1/CCR2 complex, which was based on the reported structure of receptor CXCR4 cross-linked to chemokine vMIP-II (*21*), we designed six point mutants and four double mutants at positions pointing toward the interior of the TM bundle (fig. S4 and Table 3). Each mutant was stably expressed in FlpIn human embryonic kidney (HEK) 293 cells with an N-terminal cMyc epitope tag, enabling measurement of cell surface expression. After confirming that mutant proteins were expressed in similar amounts to that of WT CCR2 (Table 3), we evaluated the affinity of chemokine binding at each mutant receptor. We extended this evaluation to measure the potency and efficacy of MCP-1 and MCP-3 at the mutant receptors using ERK1/2 phosphorylation as a convenient measurement of receptor activation that does not require the use of modified receptor fusion constructs or overexpression

Table 2. Potency, efficacy, and affinity of the chimeric MCP proteins at CCR2 in β-arrestin recruitment, ERK phosphorylation, and radioligand-binding assays. ^{125}I–MCP-1 competition binding was measured in membrane preparations of c-Myc–FLAG–CCR2 Flp-In T-REx 293 cells. β-arr2 recruitment was assessed by BRET in Flp-In T-REx 293 cells transiently transfected with plasmids encoding CCR2-RLuc8 and β-arr2–YFP. ERK1/2 phosphorylation was measured 3 to 5 min after c-Myc–FLAG–CCR2 Flp-In T-REx 293 cells were stimulated with chemokine. pEC_{50} and pK_i values are the negative log of EC_{50} and K_i values, respectively, in molar units. E_{max} values are relative to the positive control. Data are means ± SEM of three or four experiments, each performed in triplicate. *$P < 0.05$, **,^^$P < 0.01$, ***,^^^$P < 0.001$, compared to MCP-1 or MCP-3, respectively. Statistical analysis was by one-way ANOVA with Dunnett's multiple-comparison text.

	β-Arrestin recruitment		ERK1/2 phosphorylation		^{125}I–MCP-1 binding
	pEC_{50}	E_{max}	pEC_{50}	E_{max}	pK_i
MCP-1	8.00 ± 0.13	0.100 ± 0.006^^^	7.87 ± 0.32	37.8 ± 3.4	10.67 ± 0.18^^
MCP1-311	7.30 ± 0.21	0.067 ± 0.006*	6.84 ± 0.17	40.3 ± 3.2	9.90 ± 0.18
MCP1-131	8.32 ± 0.13	0.11 2 ± 0.006^^^	7.64 ± 0.26	43.7 ± 3.7	10.53 ± 0.17^^
MCP1-113	8.12 ± 0.13	0.111 ± 0.006^^^	7.58 ± 0.46	46.7 ± 6.8	10.68 ± 0.16^^
MCP1-133	8.45 ± 0.27	0.103 ± 0.009^^	7.86 ± 0.42	36.4 ± 5.0	10.84 ± 0.16^^
MCP1-333	7.82 ± 0.58	0.034 ± 0.009***	6.95 ± 0.29	24.0 ± 3.1	10.02 ± 0.17
MCP-3	7.63 ± 0.17	0.060 ± 0.004**	7.21 ± 0.31	34.3 ± 4.0	9.50 ± 0.19**
MCP3-133	8.24 ± 0.11	0.0135 ± 0.005^^^	8.12 ± 0.33	25.9 ± 2.3	10.36 ± 0.14
MCP3-313	7.17 ± 0.22	0.051 ± 0.006***	7.43 ± 0.27	33.1 ± 3.0	7.45 ± 0.23***,^^
MCP3-331	7.65 ± 0.22	0.056 ± 0.006**	7.66 ± 0.36	21.7 ± 2.3*	8.77 ± 0.33***
MCP3-311	7.13 ± 0.39	0.050 ± 0.010***	7.87 ± 0.14	40.0 ± 1.6	7.32 ± 0.32***,^^
MCP3-111	7.61 ± 0.20	0.134 ± 0.010^^^	7.99 ± 0.36	21.3 ± 2.4*	9.80 ± 0.17

of signaling effectors. None of the mutations significantly changed the affinities for MCP-1 or MCP-3 compared to that of WT CCR2 (Table 3, Fig. 4A, and fig. S5). However, comparison of the relative affinities of MCP-1 and MCP-3 at the different mutants was more revealing. MCP-3 displayed a 10-fold lower affinity for WT CCR2 than that of MCP-1. Whereas this difference in affinity was maintained in most of the CCR2 mutants, no such difference in affinity was observed with the R206A and Y259F mutants. Therefore, the difference in affinity between MCP-1 and MCP-3 appears to be governed, at least in part, by these two residues.

As shown earlier with WT CCR2, MCP-1 displayed a statistically significantly higher potency than that of MCP-3. This difference in potency was maintained across most mutants, in accordance with the relative affinities for the two ligands (Fig. 4B and fig. S5). Nevertheless, the Y259F mutant displayed increased potency for both chemokines; the double-mutant I263A/N266A displayed statistically significantly increased potency for MCP-1 ($P = 0.003$) and a smaller, but not significant, increase for MCP-3; and the D284A mutant showed a statistically significantly increased potency for MCP-1 ($P < 0.01$) but not MCP-3 (Fig. 4B). Although the potencies of ERK1/2 phosphorylation correlated well with CCR2 binding affinities for the WT chemokines (Fig. 1), there was a poor correlation between affinity and potency when comparing the same chemokine across the set of CCR2 mutants (fig. S6, A and B). This suggests that some of the mutations influenced the mechanism of receptor signaling rather than ligand binding. To further explore this possibility, we examined the maximal effects stimulated by the two chemokines in the ERK1/2 phosphorylation assay (Fig. 4C and figs. S5 and S6C). The CCR2 mutants Y120F, R206A, E270A/F272A, and E291A displayed statistically significantly lower E_{max} values for both MCP-1 and MCP-3 compared to those of WT CCR2 ($P < 0.05$). Furthermore, the maximal effect of MCP-1, but not MCP-3, was statistically significantly reduced for the I263A/N266A mutant. Conversely, the double-mutant N199A/T203A displayed a statistically significantly reduced E_{max} for MCP-3 ($P < 0.01$), but not MCP-1. Finally, the mutation K34A caused an increase in E_{max} relative to that of WT CCR2 for MCP-1, and a similar trend was observed for MCP-3. The cell surface expression of all mutants was not significantly different. Thus, these changes in maximal signaling likely reflect the roles of these residues in conformational rearrangement of CCR2 coupled to the ERK1/2 signaling pathways.

DISCUSSION

Humans and other mammals express a complex array of chemokines and chemokine receptors that collectively orchestrate the trafficking of leukocytes, a central feature of the innate immune response. The existence of multiple chemokines that activate the same receptor was previously thought to represent functional redundancy. However, some data, including observations of partial agonism (*10*–*14*) and biased agonism (*15*, *16*), increasingly suggest that different chemokines are able to alter receptor responses in a subtle and selective manner. Here, we have begun to elucidate the structural features underlying the partial agonism of MCP chemokines at their shared receptor CCR2.

Numerous previous structure-function studies of chemokines have identified residues within the N-loop and β3 region as being critical for binding interactions and residues within the N-terminal region as being

Table 3. Characterization of CCR2 mutants. Cell surface expression (receptor abundance) was measured by anti–c-Myc ELISA in c-Myc–FLAG–CCR2 Flp-In T-REx 293 cells, and data are expressed as a percentage of the abundance of the WT receptor. The affinities (pK_i) of MCP-1 and MCP-3 for WT and mutant CCR2 proteins were measured by ^{125}I–MCP-1 competition binding assays with cell membrane preparations. The potency (pEC_{50}) and efficacy (E_{max}) values of MCP-1 and MCP-3 for WT and mutant CCR2 proteins in ERK1/2 phosphorylation assays were measured 3 min after c-Myc–FLAG–CCR2 Flp-In T-REx 293 cells were stimulated with chemokine. pEC_{50} and pK_i values are the negative log of EC_{50} and K_i values, respectively, in molar units. E_{max} values are relative to the positive control. Data are means ± SEM of three or four experiments, each performed in triplicate. For radioligand binding, ^$P < 0.05$ as compared to MCP-1 for each mutant. Analysis was by multiple *t* test. For ERK1/2 phosphorylation, *$P < 0.05$, **$P < 0.01$, ***$P < 0.001$ as compared to WT CCR2. Analysis was by one-way ANOVA with Dunnett's multiple-comparison test.

Mutation	Location[#]	Cell surface expression	pK_i		pERK1/2 pEC_{50}		pERK1/2 E_{max} (% FBS)	
			MCP-1	MCP-3	MCP-1	MCP-3	MCP-1	MCP-3
WT		100 ± 3	10.82 ± 0.18	9.64 ± 0.19^	8.01 ± 0.23	7.30 ± 0.23	38.9 ± 3	35.5 ± 4.5
K34A	TM1 (1.28)	119 ± 12	10.42 ± 0.27	9.70 ± 0.42	8.41 ± 0.24	7.70 ± 0.23	55.5 ± 2.5***	45.0 ± 2.8
Y120F	TM3 (3.32)	118 ± 13	11.15 ± 0.18	9.65 ± 0.26^	7.92 ± 0.32	7.58 ± 0.33	25.4 ± 2**	16.6 ± 1.6***
V187/V189A	ECL2	108 ± 6	11.36 ± 0.29	9.85 ± 0.32^	7.99 ± 0.26	7.28 ± 0.23	30.5 ± 2	30.8 ± 2.3
N199A/T203A	TM5 (5.35/5.39)	116 ± 7	11.42 ± 0.29	10.17 ± 0.47	7.66 ± 0.23	7.35 ± 0.33	32.8 ± 2	20.2 ± 2.3**
R206A	TM5 (5.42)	112 ± 7	10.29 ± 0.22	10.12 ± 0.33	8.25 ± 0.31	7.81 ± 0.34	11.0 ± 0.8***	14.8 ± 2.5***
Y259F	TM6 (6.51)	99 ± 6	10.44 ± 0.23	10.20 ± 0.14	8.78 ± 0.36*	8.57 ± 0.26**	31.9 ± 1.7	39.3 ± 1.7
I263A/N266A	TM6 (6.55/6.58)	107 ± 8	10.79 ± 0.24	8.99 ± 0.17^	9.46 ± 0.39**	8.22 ± 0.38	24.7 ± 2***	36.9 ± 3.4
E270A/F272A	TM6/ECL3	99 ± 13	11.68 ± 0.39	10.06 ± 0.31^	7.36 ± 0.20	7.36 ± 0.20	22.3 ± 1.3***	22.1 ± 1.5**
D284A	TM7 (7.32)	104 ± 5	10.91 ± 0.16	9.52 ± 0.25^	8.83 ± 0.40**	7.80 ± 0.18	34.9 ± 2	39.1 ± 1.9
E291A	TM7 (7.39)	107 ± 9	10.26 ± 0.24	9.03 ± 0.22^	7.66 ± 0.40	7.09 ± 0.48	27.9 ± 3*	12.1 ± 2.2***

[#]Ballesteros and Weinstein numbering of TM residues is shown in parentheses (*33*).

critical for receptor activation (*26*–*29*). These conclusions are encapsulated by the two-site model, which postulates that chemokines first use their N-loop and β3 residues [chemokine site 1 (CS1)] to bind to the receptor N terminus [receptor site 1 (RS1)], and subsequently, the chemokine N terminus [chemokine site 2 (CS2)] activates the receptor by binding to its TM helices [receptor site 2 (RS2)], causing conformational changes and cellular signaling (*29*). The presumption that binding and activation occur in two discrete steps rather than concomitantly is not derived from kinetic measurements but instead deduced from indirect evidence such as the ability of N-terminally truncated chemokines to bind strongly without activating their receptors (*30*, *31*). Recent structures of two chemokine-receptor complexes (*21*, *22*) not only helped to validate key features of the two-site model but also suggested that the two sites may not be completely independent. A number of additional observations have also suggested that elaborations of the two-site model may be necessary (*32*). In summary, although the two-site model is broadly supported by structural and mutational data and has served as a useful guide for mechanistic studies, it is too simplistic to account for such subtle observations as partial or biased agonism.

The structure-function relationships of MCP-1 have been thoroughly examined in a seminal study by Handel and co-workers (*27*, *28*). MCP-1 residues Thr^{10} (N-terminal region, immediately preceding the CC motif), Tyr^{13} and Arg^{24} (N-loop), Lys^{35} ("30s" loop), and Lys^{49} (β3 region) make substantial contributions to CCR2 binding affinity, whereas the N-terminal residues Ile^{5} and Val^{9} of MCP-1 contribute to signaling through CCR2. Almost all of the MCP-1 residues shown to play key roles in CCR2 binding or activation are identical in MCP-3. Thus, the interactions of these residues are likely to also occur for MCP-3 and do not account for the differences in the CCR2 binding affinity or efficacy of MCP-1 and MCP-3. In agreement with the previous observations of MCP-1 mutants and the two-site model, our β-arr2 recruitment data for MCP1-311 and MCP3-133 indicate that the chemokine N-terminal region is the major selectivity determinant of receptor activation manifested by changes in the intrinsic efficacy of these different chemokines. However, surprisingly, our analysis of MCP-1 and MCP-3 chimeras also identified the N-terminal region as being the primary determinant of the binding selectivity of these two chemokines to CCR2. Residues within this region were not previously found to contribute to binding affinity, with the sole exception of Thr^{10} (*27*), which is identical in MCP-1 and MCP-3. Our results are consistent with the prevailing model that most of the binding affinity for both chemokines is provided by residues in the N-loop and β3 regions. However, it now appears that these regions contribute equally to the CCR2 binding affinities of both chemokines, whereas the N-terminal region of MCP-1 contributes more binding energy compared to the N-terminal region of MCP-3, resulting in the higher binding affinity of MCP-1. In the two-site model, the chemokine N-terminal region corresponds to CS2, which is considered to be the key determinant of receptor activation but not to play a role in the initial binding step. Our results suggest an extension of the two-site model such that interactions between CS2 and RS2 contribute either to the initial binding step or to the formation of a more stable complex subsequent to initial binding but before (or concomitant with) receptor activation.

To identify receptor residues that interact with the N-terminal regions of MCP-1, MCP-3, or both, we mutated residues in CCR2 whose

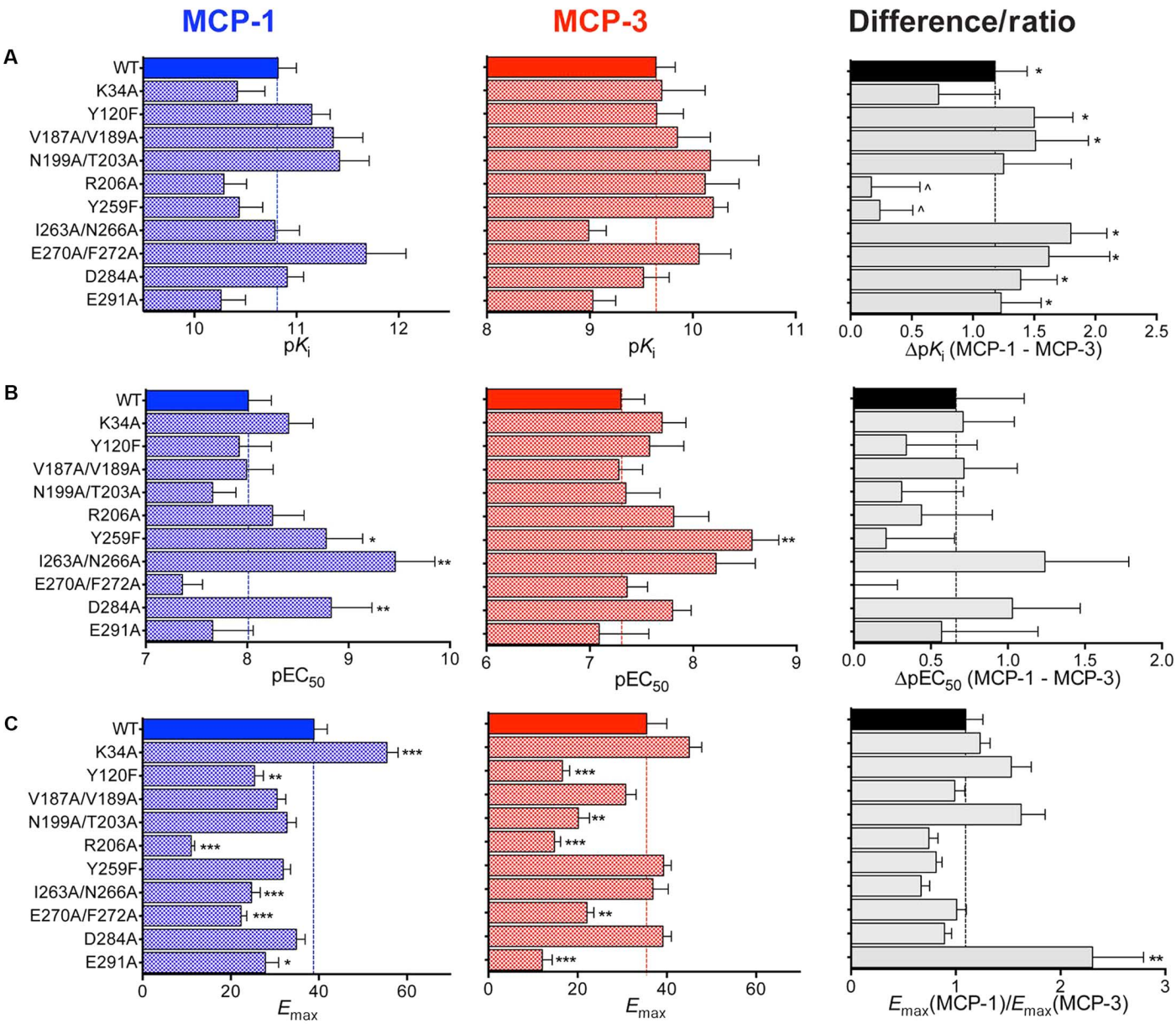

Fig. 4. Identification of CCR2 residues contributing to MCP-1 and MCP-3 binding and agonism. (**A** to **C**) ^{125}I–MCP-1 competition binding and ERK1/2 phosphorylation were assessed for MCP-1 and MCP-3 at the WT and mutant CCR2 proteins expressed in Flp-In T-REx 293 cells. (A) Membrane preparations of c-Myc–FLAG–CCR2 Flp-In T-REx 293 cells expressing WT or the indicated mutant receptors were incubated with 45 pM ^{125}I–MCP-1 in the presence of various concentrations of chemokines before the extent of binding of ^{125}I–MCP-1 was determined by radioligand-binding assay. Left: Binding affinity (pK_i) of MCP-1 for each WT and mutant receptor (blue). Middle: Binding affinity (pK_i) of MCP-3 for each WT and mutant receptor. Right: The differences between the pK_i values of MCP-1 and MCP-3 for each WT and mutant receptor (black/gray). ^$P < 0.05$, compared to the difference observed at the WT receptor;*$P < 0.05$, compared to zero (that is, indicating difference between chemokines). Analysis was by multiple *t* test. (B and C) c-Myc–FLAG–CCR2 Flp-In T-REx 293 cells were treated with various concentrations of WT or chimeric chemokines for 3 min before the amount of phosphorylated ERK1/2 was measured by AlphaScreen assay. (B) Left: Potency (pEC_{50}) of MCP-1 for each WT and mutant receptor (blue). Middle: Potency (pEC_{50}) of MCP-3 for each WT and mutant receptor (red). Right: The differences between pEC_{50} values of MCP-1 and MCP-3 for each WT and mutant receptor (gray/black). *$P < 0.05$, **$P < 0.01$ compared to the potency observed at the WT receptor, by one-way ANOVA with Dunnett's multiple-comparison test. (C) Left: Efficacy (E_{max}) of MCP-1 for each WT and mutant receptor (blue). Middle: Efficacy (E_{max}) of MCP-3 for each WT and mutant receptor (red). Right: The ratios between the E_{max} values of MCP-1 and MCP-3 for each WT and mutant receptor (gray/black). *$P < 0.05$, **$P < 0.01$, ***$P < 0.001$, ****$P < 0.0001$ compared to the values observed at the WT receptor, by one-way ANOVA with Dunnett's multiple-comparison test. Data are means ± SEM of three to five experiments, each performed in triplicate.

side chains are predicted to point toward the interior of the TM helical bundle. Several of the mutants displayed altered chemokine binding. In particular, mutation of Arg206$^{5.42}$ or Tyr259$^{6.51}$ [superscripts indicate Ballesteros-Weinstein numbering (*33*)] completely abolished the ~10-fold binding selectivity of CCR2 for MCP-1 over MCP-3. These residues form a closely packed cluster with residues Tyr120$^{3.32}$, Ile263$^{6.55}$, and Glu291$^{7.39}$ in a region where TM helices 3, 5, 6, and 7 come together, previously defined as the "major subpocket" of the receptor (Fig. 5, A to C)

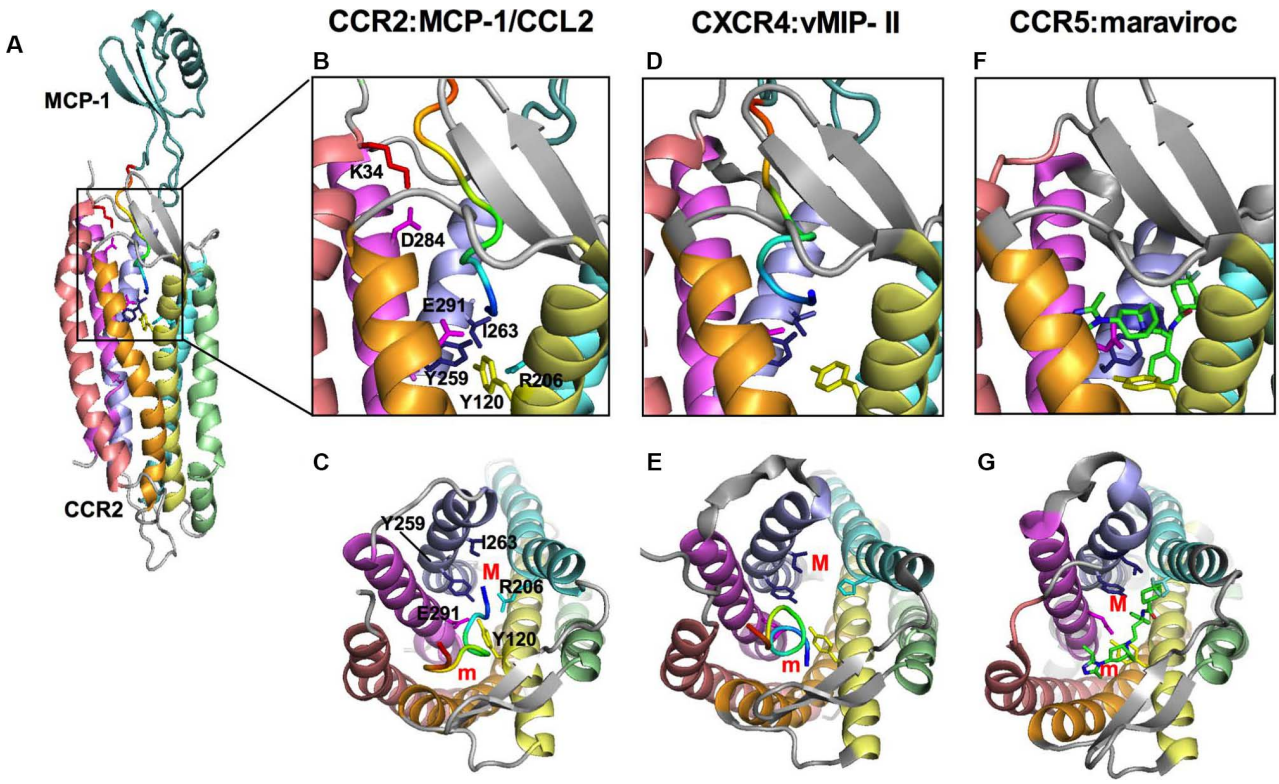

Fig. 5. The major subpocket of CCR2 recognizes the N termini of MCP chemokines. (**A** to **C**) Full (A) and detailed side views (B) and end-on view (C) (from the extracellular perspective) showing the homology model of CCR2 bound to MCP-1. CCR2 TM helices are colored salmon (TM1), orange (TM2), pale yellow (TM3), pale green (TM4), aquamarine (TM5), light blue (TM6), and violet (TM7); other receptor residues are in gray. Side chain sticks, labeled with single-letter amino acid code and residue number, are shown for several residues discussed in the text in darker shades of the same colors as the helices in which they are located. MCP-1 is in teal with the N terminus in rainbow colors from blue (residue 1) to red (residue 10). In (C), the major (M) and minor (m) subpockets are labeled in red. (**D** and **E**) The CXCR4/vMIP-II complex (PDB code: 4rws) is displayed as described for the CCR2/MCP-1 complex in (B) and (C). (**F** and **G**) The CCR5/maraviroc complex (PDB code: 4mbs) is displayed as described for the CCR2/MCP-1 complex in (B) and (C). Maraviroc is shown as sticks colored by element (carbon, green; nitrogen, blue; oxygen, red).

(*34*). In support of the contribution of this structural region to binding, mutation of Ile^{263} (in the $I263A^{6.55}/N266A^{6.58}$ double mutant) slightly reduced the affinity for MCP-3, and mutation of $Glu291^{7.39}$ slightly reduced the affinity for both MCP-1 and MCP-3 (Table 3). Although we cannot exclude the possibility that this cluster of amino acids influences chemokine binding through an indirect, allosteric mechanism, these residues are adjacent to the extreme N terminus of the bound chemokine in our homology model (Fig. 5, A to C), suggesting that they interact directly with the chemokine ligands. This conclusion is supported by an exhaustive mutagenesis study of CXCR4 defining a similar cluster of signal "initiation residues" adjacent to the N terminus of CXCL12 (*35*). Notably, in the complex of vMIP-II with CXCR4 from which our homology model was derived, the N terminus of vMIP-II points slightly away from these residues into the "minor subpocket" of CXCR4 (Fig. 5, D and E) (*21*). Our data suggest that the interactions of the CCR2 major subpocket with the chemokine N terminus play a critical role in stabilizing the chemokine-receptor complex and in determining the relative affinities of MCP-1 and MCP-3 at their shared receptor.

Among the CCR2 mutations that reduced chemokine binding affinity, the Y259F and I263A/N266A mutations surprisingly caused increased potency of MCP-1 and/or MCP-3. This lack of correlation between potency and affinity can be rationalized by considering the possible interactions of these residues in the chemokine-receptor complex before undergoing the conformational change required for activation (the inactive state) and after this conformational change (the active state). Our affinity measurements were performed in the presence of guanine nucleotides and therefore are likely to probe interactions in the (G protein–uncoupled) inactive state, whereas the potency of ERK1/2 phosphorylation is likely to be more sensitive to interactions in the active state. We suggest that the Y259F and I263A/N266A mutations disrupt interactions in the inactive state but favor the transition to the active state, thereby enhancing potency. In contrast, the R206A and E291A mutants displayed decreased affinity and decreased efficacy of ERK1/2 phosphorylation without exhibiting any statistically significant change in potency. Disruption of these residues may alter the structure of the active state such that it is no longer well coupled to ERK signaling effectors.

Several CCR2 mutations influenced ERK1/2 phosphorylation without affecting chemokine binding affinity. In particular, the $D284A^{7.32}$ mutation enhanced the potency of ERK phosphorylation in response to MCP-1, and the $K34A^{1.28}$ mutation enhanced the efficacy of ERK phosphorylation in response to either chemokine. These two residues are located adjacent to each other and form a salt bridge in our homology model (Fig. 5B). We propose that these residues do not contribute directly to ligand interactions but instead stabilize the inactive state of the receptor by interacting with each other, other residues on adjacent TM helices, or both. Disruption of these interactions may therefore facilitate the transition to the active state, albeit at the expense of destabilizing the unbound receptor structure.

In summary, we have shown that the distinct affinities and efficacies of CCR2 activation by MCP chemokines can be primarily attributed to the interactions of the chemokine N-terminal region, suggesting an elaboration of the two-site model in which the chemokine N terminus contributes to binding interactions before receptor activation occurs. By analyzing CCR2 mutants, we identified a cluster of CCR2 residues nestled between TM helices 3, 5, 6, and 7 that appears to be the key binding site for the chemokine N terminus. Considering that the equivalent residues of chemokine receptor CCR5 comprise a substantial part of the binding site for the anti-HIV drug and CCR5 inhibitor maraviroc (Fig. 5, F and G) (*36*), our results suggest that this site within CCR2 may also be a suitable target for the future development of small-molecule CCR2 inhibitors with potential applications in atherosclerosis, obesity, diabetes, and other macrophage-associated inflammatory diseases.

MATERIALS AND METHODS

Reagents

Dulbecco's modified Eagle's medium (DMEM) and Hanks' balanced salt solution (HBSS) were from Invitrogen. Blasticidin and HygroGold were from InvivoGen. Fetal bovine serum (FBS) was from In Vitro Technologies. Polyethyleneimine was from Polysciences Inc. Coelenterazine h was from NanoLight. All the other reagents were purchased from Sigma-Aldrich.

Chimeric chemokine constructs

Ten chimeras of human chemokines MCP-1 (obligate monomeric mutant P8A) and MCP-3 were designed on the basis of the aligned sequences (Fig. 2); the WT MCP-1 and all MCP-1–derived chimera used in this study contain the P8A mutation. We chose to use MCP-3 rather than MCP-2 for these chimeras for the following reasons: (i) The sequence of MCP-1 is more closely related to MCP-3 (71% identity) than to MCP-2 (61% identity), allowing us to more easily draw conclusions about the roles of specific residues. (ii) Both MCP-3 and the MCP-1(P8A) mutant used here are monomeric, whereas MCP-2 exists in equilibrium between monomeric and dimeric forms, potentially complicating the interpretation of chimera experiments if MCP-2 was used (especially in determining whether the chimeras were correctly folded). (iii) MCP-2 gives a very weak signal in the β-arr2 recruitment assay, so there may not have been a large-enough window to reliably measure any decreases in efficacy when assessing the effects of chimeras, whereas MCP-3 gives a slightly higher signal (larger window) that allows for "confident" detection of both increases and decreases in efficacy. (iv) In our expression system, MCP-3 gives a higher yield than MCP-2, so preparation of chimeras was expected to be more straightforward. Each chimera consisted of the sequence of one chemokine with one or more of the following three regions replaced by the corresponding residues from the other chemokine: N terminus (residues 1 to 10), N-loop (residues 12 to 24), and β3 region (residues 46 to 52). For N-loop substitutions, residue Val^{22} (MCP-1) and Lys^{22} (MCP-3) were not replaced, and for β3 region substitutions, residue Ile^{46} (MCP-1) and Lys^{46} (MCP-3) were not replaced because these residues are buried in the hydrophobic core, and mutation would be expected to disrupt the protein fold. Genes encoding the chimeras (with an N-terminal His-tag and modified thrombin cleavage site for tag removal) were constructed by recursive polymerase chain reaction (PCR) using overlapping oligonucleotides. The PCR products were ligated into the Nco I/Xho I (MCP-1 background) or Nco I/Bam HI (MCP-3 background) restriction sites of the pET28a plasmid and transformed into DH5α *E. coli*. Colonies containing recombinant plasmids were screened by PCR and verified by DNA sequencing. Amino acid sequences of the chemokines and chimeras are listed in fig. S7.

Chemokine expression and purification

All chemokines and chimeras were expressed and purified as described by Tan *et al.* (*37*). Briefly, the N-terminal His_6-tagged protein was expressed from BL21 (DE3) *E. coli* in LB media by induction with IPTG (isopropyl-β-D-thiogalactopyranoside). Inclusion bodies containing the fusion proteins were isolated and dissolved in denaturing buffer and then purified by Ni^{2+}-affinity chromatography. The fusion protein was refolded by dropwise dilution, the His_6-tag was removed using human thrombin, and the untagged protein (containing the native N terminus) was further purified by size exclusion chromatography. Purity was evaluated by SDS–polyacrylamide gel electrophoresis, and protein identity was confirmed by MALDI-TOF (matrix-assisted laser desorption/ionization–time-of-flight) mass spectrometry (table S3). For NMR, samples were exchanged into 20 mM sodium acetate-d_4, pH 7.0, containing 5% D_2O. ^1H NMR spectra were recorded at 25°C, referenced to external dextran sulfate sodium, on a Bruker Avance 600-MHz NMR spectrometer equipped with a triple-resonance cryoprobe and analyzed using Bruker TopSpin software.

Homology modeling of the CCR2/MCP-1 complex

To guide mutant selection, we constructed a homology model of human CCR2 bound to human MCP-1 based on the crystal structure of CXCR4 bound (and cross-linked) to the viral chemokine vMIP-II [Protein Data Bank (PDB) code: 4RWS] (*21*). Briefly, the sequences of CCR2 and CXCR4 were aligned by pairwise sequence alignment, and the program Modeller v. 9.12 (*38*) was used to construct 3D models of CCR2 based on the CXCR4 coordinates. The best CCR2 model, selected on the basis of Molpdf and high precision Discrete Optimized Protein Energy (DOPE-HR) scores, was overlaid with CXCR4, and the structure of MCP-1 (single protomer extracted from PDF file 1DOM) was overlaid with vMIP-II in the 4RWS structure. The aligned structures were then used to build a composite model of CCR2 bound to MCP-1. Chain termini were capped with neutral groups (acetyl and methylamide). Residues were protonated according to their states at pH 7. Completed structures were inserted into a palmitoyl oleoyl phosphatidyl choline (POPC) bilayer measuring 85 Å by 85 Å and then solvated in a rectangular simulation box leaving at least 46 Å of water on either side of the bilayer using the CHARMM-GUI membrane builder (*39*). System charges were neutralized with respective sodium and chloride counter ions. Proteins, ions, and lipids were modeled using the CHARMM36 Additive Force Field (*40*, *41*), and waters were represented using the three-particle TIP3P model (*42*). All bonds involving hydrogen atoms were constrained to their equilibrium lengths with the SHAKE algorithm (*43*). The resulting systems were subjected to at least 10,000 energy minimization steps to remove any clashes, followed by an equilibration protocol. During equilibration, we applied harmonic positional restraints of 10 kcal mol^{-1} $Å^{-2}$ to the protein backbone atoms, pressure was kept at 1 atm using the Berendsen algorithm (*44*), and the temperature was increased from 10 to 310 K as a linear function of time over the course of 1 ns, with Langevin temperature coupling. Relaxation time for temperature and pressure was 0.5 ps. Subsequently, we removed the restraints and performed a 5-ns simulation at constant isotropic pressure of 1 atm and temperature of 310 K. Electrostatic interactions were computed using a 10 Å cutoff radius, and the Particle Mesh Ewald

method was used for long-range interactions (*45*). All molecular dynamics (MD) simulations (equilibration and production) were carried out under periodic boundary conditions. Production simulations were carried out in the constant temperature, constant volume (NVT) ensemble. Temperature was kept at 310 K using the Langevin thermostat with a collision frequency of 2 ps. The simulation time step was 2 fs, and snapshots were taken every 100 ps. Simulations were run once with Amber 14 (D. A. Case *et al.*, University of California, San Francisco), using PMEMD on an Nvidia K20m GPU for 100 ns. The structural conformation after 100 ns was used in subsequent structural analysis.

Construction and expression of CCR2 mutants

Individual CCR2 residues or pairs of residues were selected for mutation based on their locations and orientations in the predicted chemokine binding site on the interior of the TM helical bundle. The WT c-Myc–FLAG–CCR2 construct in pcDNA5/FRT/TO (*37*) was used as a template for QuikChange site-directed mutagenesis to generate CCR2 mutants. WT and mutant c-Myc–FLAG–CCR2 constructs were transfected in HEK293 Flp-In T-REx cells using Lipofectamine (Invitrogen). Cells were selected and maintained in DMEM supplemented with 5% (v/v) tetracycline-free FBS, blasticidin (5 μg/ml), and HygroGold (200 μg/ml) at 37°C in 5% CO_2 humidified incubators. Receptor expression was induced 24 hours before each experiment by addition of tetracycline (10 μg/ml).

Determination of cell surface receptor expression by whole-cell ELISA

The cell surface expression of CCR2 was measured using anti–c-Myc ELISA as described previously (*46*). Primary antibody anti–c-Myc (9E10) was diluted (1:2000) in tris-buffered saline/0.1% (w/v) bovine serum albumin. Secondary antibody, anti–mouse–horseradish peroxidase was diluted (1:2000) in blocking buffer. Data were normalized as the ratio of OD_{490} (optical density at 490 nm) of mutants over the OD_{490} of the WT CCR2. For internalization experiments, cells were stimulated with 100 nM chemokine in full media and incubated for 1 hour at 37°C and rinsed with DMEM at pH 2.5 before fixation (*46*). All experiments were repeated at least three times and performed in triplicate.

Membrane preparation and radioligand-binding assays

Cell membranes were prepared by detaching the cells from the flasks, centrifugation at 1500*g* for 3 min, and resuspension in ice-cold 50 mM 3-(*N*-morpholino)propanesulfonic acid (Mops) buffer with 5 mM $MgCl_2$ and 0.1% 3-[(3-cholamidopropyl)-dimethylammonio]-1-propanesulfonic acid (CHAPS), pH 7.4. The lysates were homogenized by sonication and centrifuged at low speed for 5 min. Membrane and cytosolic fractions were separated by centrifugation of the supernatants at a relative centrifugal force (rcf) of 40,000*g* for 30 min. The membrane pellet was resuspended in Mops buffer with 5 mM $MgCl_2$ and 0.1% CHAPS, pH 7.4, and stored at −20°C. Protein concentrations were measured using a BCA protein determination assay (*47*). Competitive binding assays were performed as described by Zweemer *et al.* (*48*). Briefly, binding assays were performed in a 100-μl reaction volume containing 50 mM Mops buffer (pH 7.4), 5 mM $MgCl_2$, 0.1% CHAPS, 5 to 20 μg of membranes, increasing concentrations of chemokines, and 45 pM ^{125}I–MCP-1. Membranes were incubated for 120 min at 37°C. Nonspecific binding was determined in the presence of 10 μM INCB3344. Binding was terminated by dilution with ice-cold 50 mM Mops buffer supplemented with 0.05% CHAPS and 0.5 M NaCl followed by rapid filtration through a 96-well GF/C filter plate precoated with 0.5% polyethyleneimine using a PerkinElmer FilterMate Harvester (PerkinElmer). Filters were washed three times with ice-cold wash buffer and dried at 50°C, and 25 μl of MicroScint-O scintillation cocktail (PerkinElmer) was added to each well. Radioactivity was determined by using a MicroBeta^2 LumiJET 2460 Microplate Counter (PerkinElmer).

β-Arrestin recruitment assays

Recruitment of β-arr2 to CCR2 was assessed in HEK293 Flp-In T-REx transiently transfected with CCR2-RLuc8 and β-arr2–YFP as previously described (*49*). Briefly, CCR2-RLuc8 and β-arr2–YFP were transfected at a receptor/arrestin ratio of 1:4 using polyethylenimine (PEI) at a 1:6 ratio (*46*). After 24 hours, cells were replated in poly-D-lysine–coated 96-well white opaque CulturPlates (PerkinElmer). Cells were rinsed and preincubated in HBSS for 30 min at 37°C 48 hours after transfection. Coelenterazine h was added to each well (final concentration, 5 μM) followed by the immediate addition of receptor ligands. Cells were incubated further for 10 min in the dark at 37°C. Bioluminescence resonance energy transfer (BRET) measurements were obtained using a PHERAstar plate reader (BMG Labtech) that allows for sequential integration of the signals detected at 475 ± 30 and 535 ± 30 nm, using filters with the appropriate band-pass. Data are presented as a ligand-induced BRET ratio (normalized by subtracting the BRET ratio of vehicle-treated cells). All experiments were performed in triplicate and repeated independently at least three times.

ERK1/2 phosphorylation

Phosphorylation of ERK1/2 was measured using the AlphaScreen SureFire p-ERK 1/2 (Thr^{202}/Tyr^{204}) Assay Kit (PerkinElmer, TGR BioSciences) following the manufacturer's instructions. Briefly, 4×10^5 cells per well were seeded in a poly-D-lysine–coated plate in full media containing tetracycline (10 μg/ml) and serum-starved overnight. Initial time-course experiments determined that peak amounts of ERK 1/2 phosphorylation were achieved 3 min after the addition of chemokines. Therefore, for all subsequent concentration-response experiments, cells were stimulated for 3 min at 37°C. FBS (10%, v/v) was used as a positive control. The reaction was terminated by removal of the media and addition of 100 μl of SureFire lysis buffer. Cell lysis was assisted by leaving the plates on a shaker at 600 rpm for 5 min. Lysate (5 μl) was transferred to a white 384-well Proxiplate followed by the addition of 8 μl of SureFire AlphaScreen Detection Mix [240:1440:7:7 (v/v) dilution of SureFire Activation Buffer/SureFire Reaction Buffer/AlphaScreen Acceptor Beads/AlphaScreen Donor Beads]. The plate was incubated in the dark for 1.5 hours at 37°C, and the AlphaScreen signal was read on an Envision plate reader (PerkinElmer). Data were normalized between the signal in the absence of chemokine (0% response) and in the presence of 10% (v/v) FBS (100% response). All experiments were performed in triplicate and repeated independently at least three times.

Inhibition of forskolin-induced cAMP

The ability of ligands to inhibit forskolin-induced cAMP production was assessed in c-Myc–FLAG–CCR2 HEK293 Flp-In T-REx cells transiently transfected to express the CAMYEL cAMP BRET biosensor (*46*). Cells were grown overnight in white poly-D-lysine–coated 96-well CulturPlates (PerkinElmer). Transient transfection was performed using PEI at a 6:1 ratio of DNA. Forty-eight hours after transfection, cells were rinsed and preincubated in HBSS for 30 min at 37°C. Cells were then incubated with the RLuc substrate coelenterazine h (final

concentration, 5 μM) for 5 min, followed by a further 5-min incubation with increasing concentrations of chemokine. Forskolin was then added to a final concentration of 10 μM. After 5 min, the YFP and the RLuc emissions were measured using a LUMIstar Omega (BMG Labtech) that allows for sequential integration of the signals detected at 475 ± 30 and 535 ± 30 nm, using filters with the appropriate band-pass. BRET ratio was calculated as the ratio of YFP to RLuc signals, and data were expressed as the percentage of the forskolin-induced signal.

Data analysis and statistics

All data points represent the mean and error bars represent the SEM of at least three independent experiments. The results were analyzed using Prism 6.0 (GraphPad Software Inc.). All data from the concentration-response curves were normalized as outlined above and fitted using the following three parameter equation

$$Y = \text{bottom} + \frac{\text{top} - \text{bottom}}{1 + 10^{(\log \text{EC}_{50} - \log[A])}} \quad (1)$$

where top and bottom represent the maximal and minimal asymptote of the concentration-response curve, $[A]$ is the molar concentration of agonist, and EC_{50} (median effective concentration) is the molar concentration of agonist required to give a response halfway between the bottom and top. Concentration-response data were also fitted to the following form of the operational model of agonism (*23*) to allow the quantification of biased agonism

$$Y = \text{basal} + \frac{(E_m - \text{basal})\left(\frac{\tau}{K_A}\right)^n [A]^n}{[A]^n \left(\frac{\tau}{K_A}\right)^n + \left(1 + \frac{[A]}{K_A}\right)^n} \quad (2)$$

where E_m is the maximal possible response of the system, basal is the basal level of response, K_A represents the equilibrium dissociation constant of the agonist (A), and τ is an index of the signaling efficacy of the agonist that is defined as R_T/K_E, where R_T is the total number of receptors and K_E is the coupling efficiency of each agonist-occupied receptor, and n is the slope of the transducer function that links occupancy to response. The analysis assumes that the transduction machinery used for a given cellular pathway are the same for all agonists, such that the E_m and transducer slope (n) are shared between agonists. Data for all chemokines for each pathway were fit globally to determine values of K_A and τ. Biased agonism was quantified as previously described (*24*). In short, to exclude the impact of cell-dependent and assay-dependent effects on the observed agonism at each pathway, the $\log(\tau/K_A)$ value of a reference agonist, in this case MCP-1 WT, was subtracted from the $\log(\tau/K_A)$ value of the other chemokines to yield $\Delta\log(\tau/K_A)$. The relative bias was then calculated for each chemokine at the two different signaling pathways by subtracting the $\Delta\log(\tau/K_A)$ of one pathway from the other to give a $\Delta\Delta\log(\tau/K_A)$ value, which is a measure of bias. A lack of biased agonism results in values of $\Delta\Delta\log(\tau/K_A)$ not significantly different from 0 between pathways. To account for the propagation of error associated with the determination of composite parameters, the following equation was used

$$\text{Pooled\_SEM} = \sqrt{(SEj1)^2 + (SEj2)^2} \quad (3)$$

For radioligand-binding, the concentration of agonist that inhibited half of the ^{125}I–MCP-1 binding [median inhibitory concentration (IC_{50})] was determined using the following equation

$$Y = \frac{\text{Bottom} + (\text{Top} - \text{Bottom})}{1 + 10^{(X - \log \text{IC}_{50}) n_H}} \quad (4)$$

where Y denotes the percentage-specific binding, Top and Bottom denote the maximal and minimal asymptotes, respectively, IC_{50} denotes the X value when the response is midway between Bottom and Top, and n_H denotes the Hill slope factor. For ^{125}I–MCP-1 homologous competition-binding experiments, estimates of affinity (K_d) were obtained using the equation:

$$\text{IC}_{50} = [\text{Hot}] + K_d \quad (5)$$

For all other chemokines, IC_{50} values obtained from the inhibition curves were converted to K_i values using the Cheng and Prusoff equation (*50*). All affinity (pK_i), potency (pEC_{50}), and transduction ratio [$\log(\tau/K_A)$] parameters were estimated as logarithms. As we have previously demonstrated that the logarithm of the measure is approximately Gaussian (*51*), and as the application of t tests and ANOVAs assume Gaussian distribution, estimating the parameters as logarithms allows valid statistical comparison. Multiple t test comparison with Holm-Sidak correction or one-way ANOVA was used as stated in the figure legends. Significance is defined as $^*P < 0.05$, $^{**}P < 0.01$, and $^{***}P < 0.001$ for the comparison graphs.

SUPPLEMENTARY MATERIALS

www.sciencesignaling.org/cgi/content/full/10/480/eaai8529/DC1

Fig. S1. Neither MCP-2 nor MCP-3 is a biased agonist at CCR2 relative to MCP-1.
Fig. S2. NMR spectra of chemokine chimeras.
Fig. S3. MCP3-111 displays biased agonism relative to MCP-3.
Fig. S4. Homology model of CCR2 bound to MCP-1, showing the positions of the mutated residues.
Fig. S5. ^{125}I–MCP-1 competition binding and ERK1/2 phosphorylation concentration response curves for CCR2 mutants.
Fig. S6. Graphical comparisons of chemokine binding and ERK1/2 phosphorylation parameters across the set of CCR2 mutants.
Fig. S7. The amino acid sequences of MCP-1 (P8A), WT MCP-3, and the chimeric chemokines.
Table S1. Biased agonism parameters for MCP chemokines at CCR2.
Table S2. MCP3-111 displays biased agonism at CCR2 compared to MCP-3.
Table S3. Expected and observed molecular masses of WT and chimeric chemokines.

REFERENCES AND NOTES

1. T. Kenakin, A. Christopoulos, Signalling bias in new drug discovery: Detection, quantification and therapeutic impact. *Nat. Rev. Drug Discov.* **12**, 205–216 (2013).
2. T. Kenakin, Functional selectivity and biased receptor signaling. *J. Pharmacol. Exp. Ther.* **336**, 296–302 (2011).
3. W. Huang, A. Manglik, A. J. Venkatakrishnan, T. Laeremans, E. N. Feinberg, A. L. Sanborn, H. E. Kato, K. E. Livingston, T. S. Thorsen, R. C. Kling, S. Granier, P. Gmeiner, S. M. Husbands, J. R. Traynor, W. I. Weis, J. Steyaert, R. O. Dror, B. K. Kobilka, Structural insights into μ-opioid receptor activation. *Nature* **524**, 315–321 (2015).
4. A. Manglik, T. H. Kim, M. Masureel, C. Altenbach, Z. Yang, D. Hilger, M. T. Lerch, T. S. Kobilka, F. S. Thian, W. L. Hubbell, R. S. Prosser, B. K. Kobilka, Structural insights into the dynamic process of β2-adrenergic receptor signaling. *Cell* **161**, 1101–1111 (2015).
5. S. G. F. Rasmussen, B. T. DeVree, Y. Zou, A. C. Kruse, K. Y. Chung, T. S. Kobilka, F. S. Thian, P. S. Chae, E. Pardon, D. Calinski, J. M. Mathiesen, S. T. A. Shah, J. A. Lyons, M. Caffrey, S. H. Gellman, J. Steyaert, G. Skiniotis, W. I. Weis, R. K. Sunahara, B. K. Kobilka, Crystal structure of the β2 adrenergic receptor-G_s protein complex. *Nature* **477**, 549–555 (2011).
6. B. Moser, M. Wolf, A. Walz, P. Loetscher, Chemokines: Multiple levels of leukocyte migration control. *Trends Immunol.* **25**, 75–84 (2004).
7. M. Baggiolini, Chemokines in pathology and medicine. *J. Intern. Med.* **250**, 91–104 (2001).

8. C. Gerard, B. J. Rollins, Chemokines and disease. *Nat. Immunol.* **2**, 108–115 (2001).
9. A. E. I. Proudfoot, Chemokine receptors: Multifaceted therapeutic targets. *Nat. Rev. Immunol.* **2**, 106–115 (2002).
10. R. Martinelli, I. Sabroe, G. LaRosa, T. J. Williams, J. E. Pease, The CC chemokine eotaxin (CCL11) is a partial agonist of CC chemokine receptor 2B. *J. Biol. Chem.* **276**, 42957–42964 (2001).
11. A. Mueller, N. G. Mahmoud, M. C. Goedecke, J. A. McKeating, P. G. Strange, Pharmacological characterization of the chemokine receptor, CCR5. *Br. J. Pharmacol.* **135**, 1033–1043 (2002).
12. Y. Wan, J. P. Jakway, H. Qiu, H. Shah, C. G. Garlisi, F. Tian, P. Ting, D. Hesk, R. W. Egan, M. M. Billah, S. P. Umland, Identification of full, partial and inverse CC chemokine receptor 3 agonists using [^{35}S]GTPγS binding. *Eur. J. Pharmacol.* **456**, 1–10 (2002).
13. Y. A. Berchiche, S. Gravel, M. E. Pelletier, G. St-Onge, N. Heveker, Different effects of the different natural CC chemokine receptor 2b ligands on β-arrestin recruitment, $G\alpha_i$ signaling, and receptor internalization. *Mol. Pharmacol.* **79**, 488–498 (2011).
14. C. T. Veldkamp, C. Seibert, F. C. Peterson, N. B. De la Cruz, J. C. Haugner III, H. Basnet, T. P. Sakmar, B. F. Volkman, Structural basis of CXCR4 sulfotyrosine recognition by the chemokine SDF-1/CXCL12. *Sci. Signaling* **1**, ra4 (2008).
15. S. Rajagopal, S. Ahn, D. H. Rominger, W. Gowen-MacDonald, C. M. Lam, S. M. Dewire, J. D. Violin, R. J. Lefkowitz, Quantifying ligand bias at seven-transmembrane receptors. *Mol. Pharmacol.* **80**, 367–377 (2011).
16. J. Corbisier, C. Gales, A. Huszagh, M. Parmentier, J.-Y. Springael, Biased signaling at chemokine receptors. *J. Biol. Chem.* **290**, 9542–9554 (2015).
17. S. Colin, G. Chinetti-Gbaguidi, B. Staels, Macrophage phenotypes in atherosclerosis. *Immunol. Rev.* **262**, 153–166 (2014).
18. Y. Bai, Q. Sun, Macrophage recruitment in obese adipose tissue. *Obes. Rev.* **16**, 127–136 (2015).
19. S. Struyf, E. Van Collie, L. Paemen, W. Put, J. P. Lenaerts, P. Proost, G. Opdenakker, J. Van Damme, Synergistic induction of MCP-1 and –2 by IL-1beta and interferons in fibroblasts and epithelial cells. *J. Leukocyte Biol.* **63**, 364–372 (1998).
20. B. Qiu, K. A. Frait, F. Reich, E. Komuniecki, S. W. Chensue, Chemokine expression dynamics in mycobacterial (type-1) and schistosomal (type-2) antigen-elicited pulmonary granuloma formation. *Am. J. Pathol.* **158**, 1503–1515 (2001).
21. L. Qin, I. Kufareva, L. G. Holden, C. Wang, Y. Zheng, C. Zhao, G. Fenalti, H. Wu, G. W. Han, V. Cherezov, R. Abagyan, R. C. Stevens, T. M. Handel, Crystal structure of the chemokine receptor CXCR4 in complex with a viral chemokine. *Science* **347**, 1117–1122 (2015).
22. J. S. Burg, J. R. Ingram, A. J. Venkatakrishnan, K. M. Jude, A. Dukkipati, E. N. Feinberg, A. Angelini, D. Waghray, R. O. Dror, H. L. Ploegh, K. C. Garcia, Structural basis for chemokine recognition and activation of a viral G protein–coupled receptor. *Science* **347**, 1113–1117 (2015).
23. J. W. Black, P. Leff, N. P. Shankley, J. Wood, An operational model of pharmacological agonism: The effect of E/[A] curve shape on agonist dissociation constant estimation. *Br. J. Pharmacol.* **84**, 561–571 (1985).
24. T. Kenakin, C. Watson, V. Muniz-Medina, A. Christopoulos, S. Novick, A simple method for quantifying functional selectivity and agonist bias. *ACS Chem. Neurosci.* **3**, 193–203 (2012).
25. T. Kenakin, Quantifying biological activity in chemical terms: A pharmacology primer to describe drug effect. *ACS Chem. Biol.* **4**, 249–260 (2009).
26. I. Clark-Lewis, B. Dewald, M. Loetscher, B. Moser, M. Baggiolini, Structural requirements for interleukin-8 function identified by design of analogs and CXC chemokine hybrids. *J. Biol. Chem.* **269**, 16075–16081 (1994).
27. S. Hemmerich, C. Paavola, A. Bloom, S. Bhakta, R. Freedman, D. Grunberger, J. Krstenansky, S. Lee, D. McCarley, M. Mulkins, B. Wong, J. Pease, L. Mizoue, T. Mirzadegan, I. Polsky, K. Thompson, T. M. Handel, K. Jarnagin, Identification of residues in the monocyte chemotactic protein-1 that contact the MCP-1 receptor, CCR2. *Biochemistry* **38**, 13013–13025 (1999).
28. K. Jarnagin, D. Grunberger, M. Mulkins, B. Wong, S. Hemmerich, C. Paavola, A. Bloom, S. Bhakta, F. Diehl, R. Freedman, D. McCarley, I. Polsky, A. Ping-Tsou, A. Kosaka, T. M. Handel, Identification of surface residues of the monocyte chemotactic protein 1 that affect signaling through the receptor CCR2. *Biochemistry* **38**, 16167–16177 (1999).
29. M. P. Crump, J.-H. Gong, P. Loetscher, K. Rajarathnam, A. Amara, F. Arenzana-Seisdedos, J.-L. Virelizier, M. Baggiolini, B. D. Sykes, I. Clark-Lewis, Solution structure and basis for functional activity of stromal cell-derived factor-1; dissociation of CXCR4 activation from binding and inhibition of HIV-1. *EMBO J.* **16**, 6996–7007 (1997).
30. J. H. Gong, I. Clark-Lewis, Antagonists of monocyte chemoattractant protein 1 identified by modification of functionally critical NH_2-terminal residues. *J. Exp. Med.* **181**, 631–640 (1995).
31. I. Clark-Lewis, I. Mattioli, J.-H. Gong, P. Loetscher, Structure-function relationship between the human chemokine receptor CXCR3 and its ligands. *J. Biol. Chem.* **278**, 289–295 (2003).
32. A. B. Kleist, A. E. Getschman, J. J. Ziarek, A. M. Nevins, P.-A. Gauthier, A. Chevigne, M. Szpakowska, B. F. Volkman, New paradigms in chemokine receptor signal transduction: Moving beyond the two-site model. *Biochem. Pharmacol.* **114**, 53–68 (2016).
33. J. A. Ballesteros, H. Weinstein, in *Methods in Neurosciences*, vol. 25, S. C. Sealfon, Ed. (Academic Press, 1995), pp. 366–428.
34. L. Roumen, D. J. Scholten, P. de Kruijf, I. J. P. de Esch, R. Leurs, C. de Graaf, C(X)CR in silico: Computer-aided prediction of chemokine receptor–ligand interactions. *Drug Discov. Today Technol.* **9**, e281–e291 (2012).
35. M. P. Wescott, I. Kufareva, C. Paes, J. R. Goodman, Y. Thaker, B. A. Puffer, E. Berdougo, J. B. Rucker, T. M. Handel, B. J. Doranz, Signal transmission through the CXC chemokine receptor 4 (CXCR4) transmembrane helices. *Proc. Natl. Acad. Sci. U.S.A.* **113**, 9928–9933 (2016).
36. Q. Tan, Y. Zhu, J. Li, Z. Chen, G. W. Han, I. Kufareva, T. Li, L. Ma, G. Fenalti, W. Zhang, X. Xie, H. Yang, H. Jiang, V. Cherezov, H. Liu, R. C. Stevens, Q. Zhao, B. Wu, Structure of the CCR5 chemokine receptor–HIV entry inhibitor maraviroc complex. *Science* **341**, 1387–1390 (2013).
37. J. H. Y. Tan, M. Canals, J. P. Ludeman, J. Wedderburn, C. Boston, S. J. Butler, A. M. Carrick, T. R. Parody, D. Taleski, A. Christopoulos, R. J. Payne, M. J. Stone, Design and receptor interactions of obligate dimeric mutant of chemokine monocyte chemoattractant protein-1 (MCP-1). *J. Biol. Chem.* **287**, 14692–14702 (2012).
38. N. Eswar, B. Webb, M. A. Marti-Renom, M. S. Madhusudhan, D. Eramian, M.-y. Shen, U. Pieper, A. Sali, Comparative protein structure modeling using MODELLER. *Curr. Protoc. Bioinformatics* **5**, Unit-5.6 (2006).
39. S. Jo, J. B. Lim, J. B. Klauda, W. Im, CHARMM-GUI membrane builder for mixed bilayers and its application to yeast membranes. *Biophys. J.* **97**, 50–58 (2009).
40. J. Huang, A. D. MacKerell Jr., CHARMM36 all-atom additive protein force field: Validation based on comparison to NMR data. *J. Comput. Chem.* **34**, 2135–2145 (2013).
41. J. B. Klauda, R. M. Venable, J. A. Freites, J. W. O'Connor, D. J. Tobias, C. Mondragon-Ramirez, I. Vorobyov, A. D. MacKerell Jr., R. W. Pastor, Update of the CHARMM all-atom additive force field for lipids: Validation on six lipid types. *J. Phys. Chem. B* **114**, 7830–7843 (2010).
42. W. L. Jorgensen, J. Chandrasekhar, J. D. Madura, R. W. Impey, M. L. Klein, Comparison of simple potential functions for simulating liquid water. *J. Chem. Phys.* **79**, 926–935 (1983).
43. R. A. Lippert, K. J. Bowers, R. O. Dror, M. P. Eastwood, B. A. Gregersen, J. L. Klepeis, I. Kolossvary, D. E. Shaw, A common, avoidable source of error in molecular dynamics integrators. *J. Chem. Phys.* **126**, 046101 (2007).
44. H. J. C. Berendsen, J. P. M. Postma, W. F. Vangunsteren, A. Dinola, J. R. Haak, Molecular-dynamics with coupling to an external bath. *J. Chem. Phys.* **81**, 3684–3690 (1984).
45. T. Darden, D. York, L. Pedersen, Particle mesh Ewald: An $N\cdot\mathrm{Log}(N)$ method for Ewald sums in large systems. *J. Chem. Phys.* **98**, 10089–10092 (1993).
46. D. J. Scholten, M. Canals, M. Wijtmans, S. de Munnik, P. Nguyen, D. Verzijl, I. J. de Esch, H. F. Vischer, M. J. Smit, R. Leurs, Pharmacological characterization of a small-molecule agonist for the chemokine receptor CXCR3. *Br. J. Pharmacol.* **166**, 898–911 (2012).
47. P. K. Smith, R. I. Krohn, G. T. Hermanson, A. K. Mallia, F. H. Gartner, M. D. Provenzano, E. K. Fujimoto, N. M. Goeke, B. J. Olson, D. C. Klenk, Measurement of protein using bicinchoninic acid. *Anal. Biochem.* **150**, 76–85 (1985).
48. A. J. M. Zweemer, I. Nederpelt, H. Vrieling, S. Hafith, M. L. Doornbos, H. de Vries, J. Abt, R. Gross, D. Stamos, J. Saunders, M. J. Smit, A. P. Ijzerman, L. H. Heitman, Multiple binding sites for small-molecule antagonists at the CC chemokine receptor 2. *Mol. Pharmacol.* **84**, 551–561 (2013).
49. M. A. Ayoub, Y. Zhang, R. S. Kelly, H. B. See, E. K. M. Johnstone, E. A. McCall, J. H. Williams, D. J. Kelly, K. D. G. Pfleger, Functional interaction between angiotensin II receptor type 1 and chemokine (C-C motif) receptor 2 with implications for chronic kidney disease. *PLOS ONE* **10**, e0119803 (2015).
50. C. Yung-Chi, W. H. Prusoff, Relationship between inhibition constant (K_i) and concentration of inhibitor which causes 50 per cent inhibition (I_{50}) of an enzymatic-reaction. *Biochem. Pharmacol.* **22**, 3099–3108 (1973).
51. A. Christopoulos, Assessing the distribution of parameters in models of ligand–receptor interaction: To log or not to log. *Trends Pharmacol. Sci.* **19**, 351–357 (1998).

Acknowledgments: We thank H. Yeatman and J. Ludeman for technical assistance.
Funding: This study was supported by the Australian Research Council Discovery Grant DP120100194, the Linkage Infrastructure, Equipment and Facilities (LIEF) grant LE0989504 (M.J.S.), Monash Institute of Pharmaceutical Sciences Large Grant Support Scheme (M.C.), and ANZ Trustees grant 12-3831 (M.J.S. and M.C.). K.D.G.P. is a National Health and Medical Research Council (NHMRC) RD Wright Career Development Fellow (1085842), and J.R.L. is a Monash University Larkins Fellow and an RD Wright Career Development Fellow. M.C. is a Monash Fellow. **Author contributions:** Z.E.H. and J.S. participated in the research design and performed the experiments. H.D.L. performed and supervised the radioligand-binding assays. J.L.B. generated the preliminary data. C.H. performed and interpreted the mass spectrometry. B.J.P. and B.T.P. generated the homology models. J.G.P. contributed to the chimera design and preparation. K.D.G.P. provided the CCR2-RLuc8 construct for BRET assays. J.R.L., M.C., and M.J.S. interpreted the results and wrote the manuscript. M.C. and M.J.S. conceived the studies and designed the experiments. All authors read and critically reviewed the manuscript. **Competing interests:** The authors declare that they have no competing interests.

Submitted 22 August 2016
Accepted 5 May 2017
Published 23 May 2017
10.1126/scisignal.aai8529

Citation: Z. E. Huma, J. Sanchez, H. D. Lim, J. L. Bridgford, C. Huang, B. J. Parker, J. G. Pazhamalil, B. T. Porebski, K. D. G. Pfleger, J. R. Lane, M. Canals, M. J. Stone, Key determinants of selective binding and activation by the monocyte chemoattractant proteins at the chemokine receptor CCR2. *Sci. Signal.* **10**, eaai8529 (2017).

Key determinants of selective binding and activation by the monocyte chemoattractant proteins at the chemokine receptor CCR2

Zil E. Huma, Julie Sanchez, Herman D. Lim, Jessica L. Bridgford, Cheng Huang, Bradyn J. Parker, Jiann G. Pazhamalil, Benjamin T. Porebski, Kevin D. G. Pfleger, J. Robert Lane, Meritxell Canals and Martin J. Stone (May 23, 2017)

Science Signaling **10** (480), . [doi: 10.1126/scisignal.aai8529]